Environmental Science & Technology

Article

pubs.acs.org/est

Divergent Aquifer Biogeochemical Systems Converge on Similar and Unexpected Cr(VI) Reduction Products

Harry R. Beller,[†] Li Yang,[†] Charuleka Varadharajan,[†] Ruyang Han,[†] Hsiao Chien Lim,[†] Ulas Karaoz,[†] Sergi Molins,[†] Matthew A. Marcus,[‡] Eoin L. Brodie,[†] Carl I. Steefel,[†] and Peter S. Nico*[,†]

[†]Earth Sciences Division and [‡]Advanced Light Source, Lawrence Berkeley National Laboratory, Berkeley, California 94720, United States

Supporting Information

ABSTRACT: In this study of reductive chromium immobilization, we found that flow-through columns constructed with homogenized aquifer sediment and continuously infused with lactate, chromate, and various native electron acceptors diverged to have very different Cr(VI)-reducing biogeochemical regimes characterized by either denitrifying or fermentative conditions (as indicated by effluent chemical data, 16S rRNA pyrotag data, and metatranscriptome data). Despite the two dramatically different biogeochemical environments that evolved in the columns, these regimes created similar Cr(III)−Fe(III) hydroxide precipitates as the predominant Cr(VI) reduction product, as characterized by micro-X-ray fluorescence and micro-X-ray absorption near-edge structure analysis. We discuss two conflicting scenarios of microbially mediated formation of Cr(III)−Fe(III) precipitates, each of which is both supported and contradicted by different lines of evidence: (1) enzymatic reduction of Cr(VI) to Cr(III) followed by coprecipitation of Cr(III) and Fe(III) and (2) both regimes generated at least small amounts of Fe(II), which abiotically reduced Cr(VI) to form a Cr−Fe precipitate. Evidence of zones with different levels of Cr(VI) reduction suggest that local heterogeneity may have confounded interpretation of processes based on bulk measurements. This study indicates that the bulk redox status and biogeochemical regime, as categorized by the dominant electron-accepting process, do not necessarily control the final product of Cr(VI) reduction.

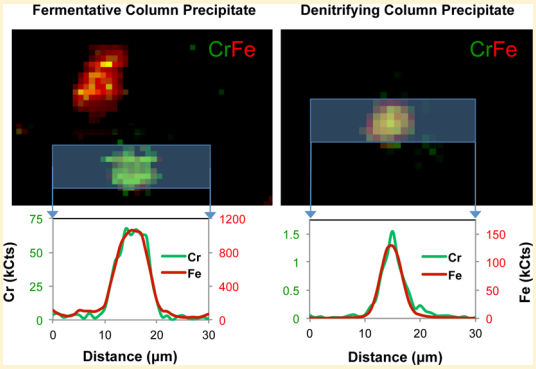

INTRODUCTION

Chromium is a potent toxin, mutagen, and carcinogen[1,2] that is a common groundwater contaminant at industrial sites in the U.S.[3] and worldwide. Cr has two commonly observed oxidation states under relevant natural conditions: Cr(VI), which exists as the highly soluble oxyanion CrO_4^{2-}, and Cr(III), which is poorly soluble and readily precipitates as either $Cr(OH)_3$ or as mixed Fe−$Cr(OH)_3$. Owing to the low solubility and mobility of reduced Cr in groundwater, *in situ* reductive immobilization of chromate plumes is considered an attractive remediation strategy.

Microbially mediated chromate reduction has been reported under a range of electron-accepting conditions, some of which produce respiration products [such as Fe(II) or hydrogen sulfide] that increase the probability of secondary abiotic Cr(VI) reduction. Diverse aerobic, facultative, and anaerobic bacteria have been reported to reduce Cr(VI) enzymatically,[4] but only for a relatively small subset of known chromate-reducing bacteria have the proteins catalyzing Cr(VI) reduction been identified and characterized biochemically, as reviewed elsewhere.[4,5] Among common abiotic reductants of Cr(VI), Fe(II) is the most efficient. A comparison of Cr(VI) reduction rates studied under a range of conditions (pH 2−9) with environmentally relevant concentrations of potential reductants including Fe(II) (30 μM), hydrogen sulfide (10 μM), soil fulvic acid, phenol, and magnetite (specific surface area, 23.8 ± 0.1 m^2/g) showed that at pH > 5.5, Fe(II) kinetically outcompeted the other potential abiotic reductants.[6]

The long-term effectiveness of *in situ* immobilization as a remediation strategy depends to a large extent on the stability of the reduced Cr once ambient (oxidized) geochemical conditions become re-established after biostimulation. It is known that Cr(III) can be reoxidized to Cr(VI) via reaction with Mn oxides. The rate at which this process will occur is likely dependent on the form of the solid-phase Cr present; however, Cr(III) oxidation via insoluble phases interacting with Mn oxides is relatively fast.[7−9] For this reason, the pathways by which Cr is reduced, and therefore the different products formed, could have a significant impact on the longevity of the remediation intervention.

Under actual field conditions, the mechanism responsible for the reduction of Cr(VI) is difficult to observe or predict given the complexity of the indigenous microbial community and the

Received: April 6, 2014
Revised: July 7, 2014
Accepted: August 1, 2014

   dx.doi.org/10.1021/es5016982 | Environ. Sci. Technol. XXXX, XXX, XXX−XXX

variety of available electron acceptors. The Hanford 100H aquifer (Washington) has a range of potential dissolved and solid-phase electron acceptors that the indigenous microbial community can use in succession.[10] In this paper, we describe studies of flow-through columns constructed with Hanford 100H aquifer sediment and continuously infused with lactate and chromate that diverged to have different biogeochemical regimes (i.e., prevalent electron-accepting conditions), namely denitrifying and fermentative conditions. We report here that despite the two dramatically different biogeochemical environments that evolved in the columns, neither of which is dominated by microbially mediated Fe(III) reduction, these regimes produced very similar Cr−Fe hydroxide precipitates as the predominant Cr(VI) reduction product.

EXPERIMENTAL SECTION

Construction and Maintenance of Hanford 100H Flow-through Columns. Flow-through column experiments were conducted with homogenized sediments from the Hanford Formation (Hanford 100H site in Washington state; Well 699-96-45 borehole intervals 41.5′ to 42′ bgs and 43.5′ to 44.0′ bgs). Briefly, the sand fraction of the Hanford formation sediment consists of quartz, plagioclase, hornblende, and mica (muscovite, biotite) with minor magnetite, orthoclase, and ilmenite, whereas the clay and silt fractions contain micas, vermiculite, chlorite (clinochlore), and ferruginous biedellite.[11] Columns were constructed by packing sediment in 6 mL, sterile, solid-phase extraction cartridges [7.8 cm (L) × 0.64 cm (i.d.)] with Luer fittings on both sides connected to autoclaved Tygon tubing for delivery of injection and effluent solutions. Three different conditions were used for incubation: (1) no electron acceptor added—3 columns, (2) nitrate-amended—5 columns, and (3) sulfate-amended—6 columns. Simulated Hanford groundwater (prepared anaerobically) was pumped through the columns at 3 μL/min (in upflow mode) by a 24-channel syringe pump. Three groundwater compositions were used that were modeled on native groundwater but differed in the electron acceptor added. All synthetic groundwater compositions contained the following basal constituents: 5 μM Cr(VI), 5 mM sodium lactate, 1.25 mM sodium bicarbonate, 1 mM potassium phosphate buffer (pH 7), 1.6 mM calcium chloride, and 0.1 mM ammonium chloride. This synthetic groundwater was used for "no electron acceptor added" columns. Nitrate-amended groundwater was basal groundwater with 12 mM potassium nitrate, and sulfate-amended groundwater was basal groundwater with 7.5 mM magnesium sulfate added. Highly purified water (18 MΩ resistance) obtained from a Milli-Q Biocel system (Millipore, Bedford, MA) was used to prepare the synthetic groundwater and all other aqueous solutions described in this article. The columns were stored in an anaerobic glovebox with an ultra high-purity N_2 atmosphere. Tracer tests with bromide were performed on all columns before incubation with the test solutions. Regular sampling was conducted of effluent that was passed through 0.2-μm sterile filters. Filtered effluent was analyzed for multiple variables, including: lactate, acetate, pyruvate, nitrate, nitrite, sulfate, and chloride (by ion chromatography[12]), and soluble Cr, Mn, and Fe (by inductively coupled plasma-mass spectrometry, or ICP-MS[12]). Concentrations of Cr, Mn, and Fe detected after filtration were assumed to be approximately equivalent to those of Cr(VI), Mn(II), and Fe(II), respectively, based on the poor solubility of the other oxidation states of these metals. At selected times, certain columns were sacrificed for solid-phase chemical and X-ray absorption spectroscopy (XAS) analysis. Sacrificial sampling was conducted by sectioning the column length-wise into three approximately equal portions in an anaerobic glovebox. Sediments used for biological analysis were immediately preserved in an RNA preservation reagent (25 mM sodium citrate, 10 mM EDTA, 10 M ammonium sulfate, pH 5.2[13]), while sediments used for chemical and spectroscopic analysis were allowed to dry in the glovebox. Occasionally, unfiltered effluent was sampled for phylogenetic (16S rRNA gene) and metatranscriptomic analysis (by custom gene-expression microarrays). Effluents (15 mL) were collected directly into 50 mL tubes containing 30 mL of the RNA preservation reagent. After overnight incubation at 4 °C, the solution was filtered (0.22-μm pore size) and DNA and RNA was coextracted from filter sections using a modification of the extraction procedure reported by Ivanov and co-workers.[14]

Solid-State Chemical Analyses for Fe(II) and Cr. Extractable Cr and Fe in the selected column sections and untreated aquifer sediments were measured by adding 10 mL of 0.5 N HCl to 0.5 g of air-dried sediment for 1 h (for samples harvested after 12 months of incubation), and 1 mL of 0.5 N HCl to 1 g of sediment for 6 h (for samples harvested after 3 months) in an anaerobic glovebox.[15] Total Cr and Fe concentrations were determined using ICP−MS, and Fe(II) was measured spectrophotometrically with ferrozine.[16]

X-ray Absorption Spectroscopic Analyses. Micro-XRF (X-ray fluorescence) maps and XANES (X-ray absorption near edge structure) spectra were collected for column sediments and lab-synthesized standards at beamline 10.3.2 of the Advanced Light Source (ALS) under standard operating conditions. Sediment samples were dusted onto Kapton tape and placed on Al sample holders. Chromium hotspots were identified by XRF mapping, usually at 10 keV, and the XANES spectra were collected at identified hotspots. Usually XANES were collected in Quick-XAS mode to reduce the potential for unrecognized beam damage and loss of signal due to sample movement. ATHENA[17] was used for XANES data reduction and spectral comparison. Images of fine-resolution XRF maps and the associated fluorescence Cr and Fe profiles were generated using 10.3.2-specific software developed by Matthew Marcus.

Pyrosequencing of Microbial Communities in Column Effluents. From DNA extracts obtained from column effluents and three destructively sampled column sediment sections, the 16S rRNA gene was amplified, purified, sequenced by pyrosequencing, and analyzed using a QIIME[18] workflow as described previously.[19] Using OTU tables generated from the QIIME workflow, Bray−Curtis distance matrices were calculated and hierarchical cluster analysis performed to display relative distance between samples based on the relative abundances of organisms detected. After data processing in QIIME, all further statistical analyses of the pyrotag data was performed in the R Statistical Programming Environment.[20]

Metatranscriptomic Analysis of Microbial Communities Using Custom Gene-Expression Microarrays. Column effluent samples collected between days 280 and 300 were analyzed for metatranscriptome (community gene expression) profiles. Total RNA (50 ng) from the samples was amplified, labeled, hybridized to custom NimbleGen arrays (described below), washed, and scanned as described previously.[21] Data from NimbleGen array scans were analyzed by building a custom array annotation package with the R *makePdInfoPackage*

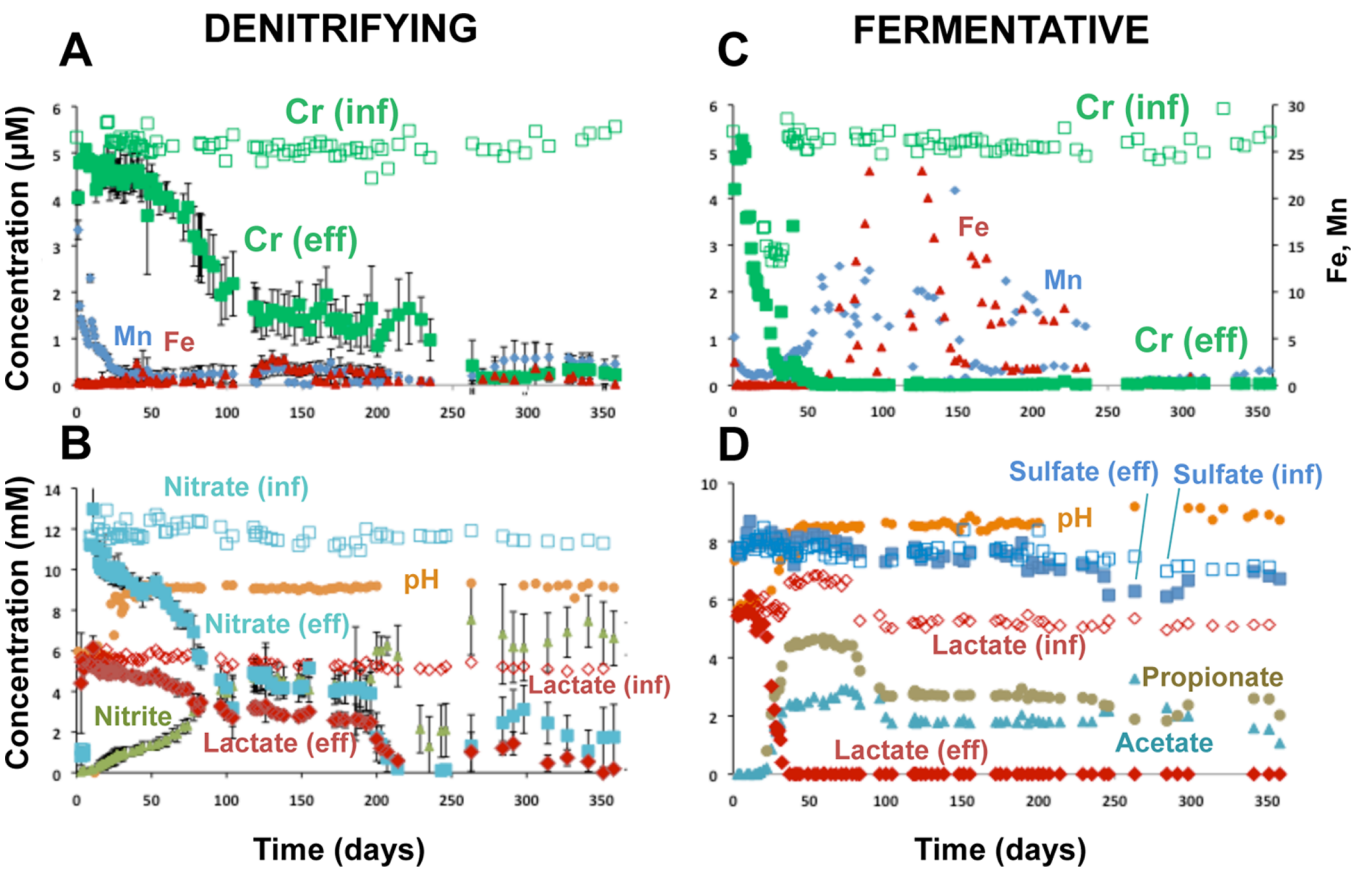

Figure 1. Effluent and selected influent data for denitrifying (A and B) and fermentative (C and D) flow-through columns with Hanford 100H aquifer sediment. Unless the labels "eff" (effluent) and "inf" (influent) are shown for a given chemical, the data represent effluent data. For denitrifying columns, the mean ± standard deviation for five columns is shown, and for fermentative columns, data for one of the two fermentative columns are shown. Effluent data were similar for the two fermentative columns, but data for only one column are plotted for better readability of the graphs. Individual data for all replicate columns are presented in Supporting Information, Figure S1 (denitrifying columns) and Figure S3 (fermentative columns).

function and normalizing probe-level data using the Robust Multiarray Average (RMA) approach with the R *rma* function available in Bioconductor, *pdInfoBuilder*, and *oligo* libraries, respectively. Normalized probe level data were summarized into gene expression values using the R *exprs* function.

As described in more detail in the Supporting Information, a custom microarray (6 × 630 K format)(Roche NimbleGen, Inc., Madison, WI) was designed to analyze gene expression of Hanford 100H aquifer microbial communities under conditions relevant to chromate reductive immobilization with lactate as the electron donor. Briefly, microarray probes were based on the predicted open reading frames (ORFs) from genomes of three Hanford 100H bacterial isolates that catalyze chromate reduction (*Pelosinus* sp. strain HCF1,[13] *Pseudomonas* sp. strain HCN1, and *Desulfosporosinus* sp. strain HCS1) and 12 metagenomes from various Hanford 100H experimental systems, including denitrifying and fermentative columns (described here) and groundwater samples from field tests involving lactate injection.

Microarray data have been deposited in the Gene Expression Omnibus (GEO) database (http://www.ncbi.nlm.nih.gov/geo) under accession number GSE56554.

RESULTS AND DISCUSSION

Effluent Chemical Data from Denitrifying and Fermentative Biogeochemical Regimes. Despite all columns starting with the same inoculum (homogenized Hanford 100H aquifer sediment), they evolved to have very different biogeochemical regimes, in large part as a result of different electron acceptors that were supplied in the influent. We focus here on the columns that were most efficient at chromate removal, namely, columns that evolved to denitrifying or fermentative biogeochemical regimes.

All five columns receiving influent containing 12 mM nitrate (in addition to 5 mM lactate and 5 μM chromate) readily showed evidence of nitrate reduction and lactate consumption that continued throughout the approximately 12-month experiment (average effluent data shown in Figures 1A,B; individual column effluent data shown in Supporting Information, Figures S1A–S1J). Over the first 100 days of incubation, all nitrate-amended columns showed a monotonic decrease in lactate, nitrate, and chromate concentration and an increase in nitrite concentration (Figure 1A,B). Nitrate consumption and nitrite accumulation were highly correlated over this period (r^2 = 0.956). By day 100, the amount of nitrate consumed exceeded nitrite accumulation by more than 3 mM, suggesting further reduction of nitrite via denitrification (confirmed by metatranscriptomic data, discussed below). After day 200, lactate, nitrate, and chromate consumption became more complete; however, the concentration decreases were less monotonic. Accumulation of pyruvate (a lactate oxidation product) was evident in column effluent, and reached

dx.doi.org/10.1021/es5016982 | Environ. Sci. Technol. XXXX, XXX, XXX–XXX

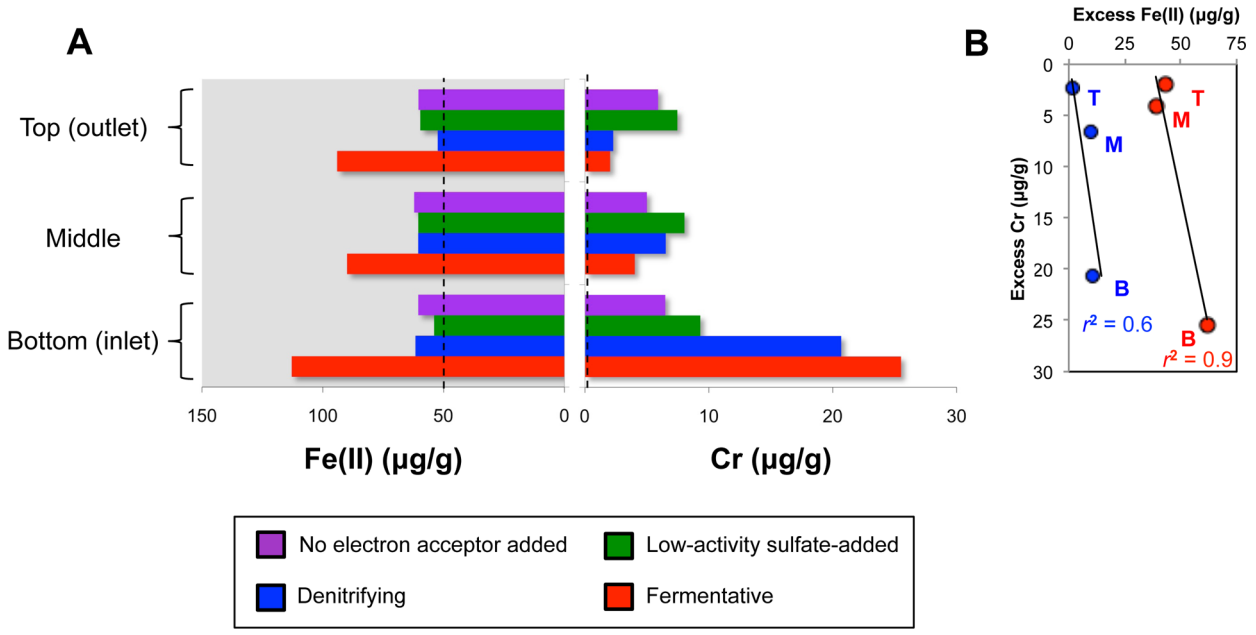

Figure 2. Fe(II) and Cr extracted (0.5 N HCl) from aquifer sediments after approximately one year of operation. (A) Concentrations (per g sediment) for three longitudinal segments of columns from all four observed biogeochemical regimes and (B) scatterplots of excess Cr vs excess Fe(II) (where "excess" signifies concentration after subtracting background value) for a denitrifying column (blue) and fermentative column (red) for the three longitudinal segments (B = bottom; M = middle; T = top). In panel A, the black dashed lines represent background values for samples of the homogenized aquifer sediment that were never operated in flow-through mode.

concentrations as high as 4 mM (data not shown). Fe and Mn were sometimes detected in column effluent, but concentrations rarely exceeded 1 μM (Figure 1A).

A noteworthy finding in the nitrate-fed columns was the relatively strong correlation observed between chromate reduction and nitrate reduction over the first 100 days (r^2 = 0.81; n = 27; Supporting Information, Figure S2). This correlation is consistent with that observed during chromate reduction that was cometabolic with nitrate reduction in a lactate-utilizing, denitrifying isolate (*Pseudomonas* sp. strain RCH2) from Hanford 100H.[12] Although the correlation itself does not demonstrate that chromate reduction was cometabolic with nitrate reduction in the columns, it is clearly not what would be expected if nitrate and chromate were acting as competing electron acceptors used sequentially, as has been observed in other denitrifying cultures.[22]

Of the six columns that were exposed to influent containing 7.5 mM sulfate, two effectively depleted the influent lactate (5 mM) and chromate (5 μM) consistently after day 40 (Figure 1C,D and Supporting Information, Figure S3A–D) and were thus much more efficient at chromate reduction than the denitrifying columns. These two columns produced acetate and propionate as lactate fermentation products; the ratio of propionate:acetate observed in these columns (averaging ~1.65 over the first 200 days) was similar to the ratio of 2.0 observed for the fermentative isolate *Pelosinus* sp. strain HCF1,[13] which predominated the microbial communities in these two columns (discussed below). (Note that the upward excursion in propionate and acetate effluent concentrations between days ~40 and 75 corresponded to an inadvertently higher lactate concentration in the influent during this time.) Sulfate reduction (relative to influent concentrations) was not detectable for the first 200 days and never became a dominant process in any sulfate-fed columns. Fe and Mn concentrations in the effluent varied over time and never exceeded ~25 μM (Figure 1C and Supporting Information, Figure S3A–B).

Chromate reduction was also observed in the remaining four sulfate-fed columns (Figure S4) although to a lesser extent or with a later onset than the two columns just described. Similarly, the columns with no electron acceptor present other than native Fe(III) minerals had relatively low levels of lactate and chromate consumption (Figure S5).

Solid-Phase Chemical Data from All Biogeochemical Regimes. Figure 2A shows acid-extractable Fe(II) and Cr in aquifer sediment recovered from the four different column types at the end of the year-long experiment: denitrifying (effluent data in Figure S1A,F), fermentative (Figure S3A,C), low-activity sulfate-added (Figure S4A,E), and no-electron-acceptor-added (Figure S5A,D). In the most active columns (i.e., denitrifying and fermentative), the amounts of Cr deposited in the solid state markedly exceeded background levels (Figure 2B). This "excess Cr" was concentrated toward the inlet (i.e., bottom, as the columns were run in upflow mode), reflecting zonation along even the short column length and consistent with the observed depletion of Cr in the effluent solutions. For the lower activity columns, there was still Cr deposited in the columns well above background levels, but there was less variation along the length of the columns. Analogous data from columns sacrificed at 3 months (rather than 12 months) reveal that all column types tested had comparable Cr concentrations at the inlet (from 1.7 to 2.1 μg/g for denitrifying, low-activity sulfate-fed, and no-electron-acceptor-added columns; fermentative columns were not tested at 3 months; Figure S6). Between 3 and 12 months, extractable Cr at the column inlet increased ~20-fold for the denitrifying columns, but only 3- to 4-fold for the low-activity sulfate-amended and no-electron-acceptor-added columns (Figure S6), reflecting that the Cr(VI) reduction rate increased in the

dx.doi.org/10.1021/es5016982 | Environ. Sci. Technol. XXXX, XXX, XXX–XXX

denitrifying columns (Figure 1A) but was relatively constant in the lower activity columns.

The acid-extractable Fe(II) values also showed variation with distance along the column (Figure 2A). All three sections of the fermenting column had Fe(II) values exceeding the background level ["excess Fe(II)"], with the largest value at the column inlet. Although acid-extractable Fe(II) concentrations exceeding background levels are most clear for the fermentative columns, the other three column types had Fe(II) concentrations exceeding background levels by 10 to 20%; statistical *P*-values for differences from the background level ranged from 0.001 to 0.1. For the fermentative and denitrifying columns, there were moderately strong linear correlations between excess Fe(II) and excess Cr deposited (Figure 2B), with r^2 values of 0.9 and 0.6, respectively. Possible mechanisms that might lead to a correspondence between Cr and Fe(II) are discussed later.

Phylogenetic and Metatranscriptomic Data from Denitrifying and Fermentative Biogeochemical Regimes. For both column sediment and effluents, we observed strong evidence of dramatic divergence in the phylogenetic composition of bacteria that inhabited the columns under nitrate-fed (denitrifying) versus fermentative conditions. 16S rRNA gene pyrotag results are presented in Figure 3 for

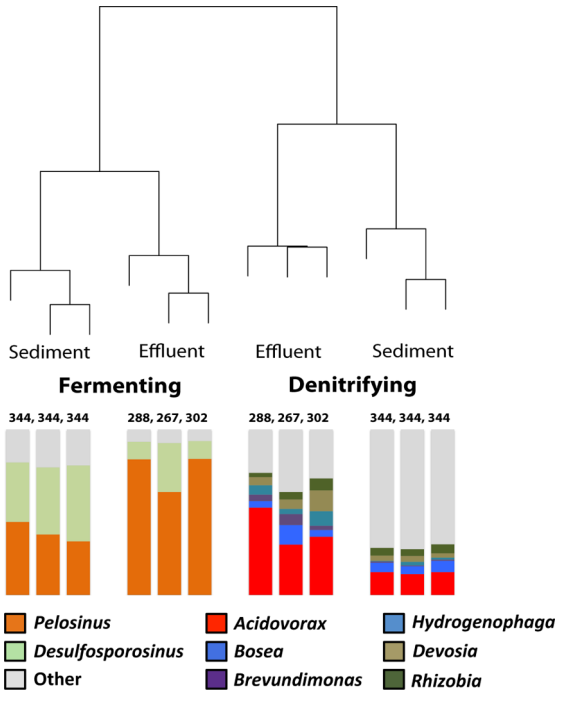

Figure 3. Hierarchical cluster plots showing the divergent microbial composition (based on the 16S rRNA gene) between columns under bulk denitrifying and fermentative conditions for both effluent and sediment phases. Bar plots under each leaf of the tree show the distributions of the most abundant organisms and numbers directly above the bars represent sampling dates (in elapsed days since the experiment started).

unfiltered effluent samples collected between days 267 and 302 and destructively sampled sediments taken at day 344 (at the conclusion of the experiment). Pyrotag analyses indicate that the differences in the species composition between the columns under different regimes were mostly due to denitrifying bacteria (*β*-Proteobacteria belonging to *Acidovorax* and *Hydrogenophaga* and *α*-Proteobacteria belonging to *Bosea, Brevundimonas, Devosia*, and *Rhizobia*) in the denitrifying columns, whereas fermentative columns were dominated by Firmicutes (in particular, *Pelosinus* sp. strain HCF1[13]). Although sulfate-reducing activity was low in the fermentative columns (noted previously), sulfate-reducing species also capable of fermentation (such as *Desulfosporosinus* spp.) were also occasionally abundant, particularly in sediment samples. As the influent solutions for the columns were autoclaved and also passed through 0.2-*μ*m prefilters before entering the columns, the homogenized aquifer sediments in the columns were the sole inoculum source. Thus, the dramatically different microbial communities that evolved in the denitrifying and fermentative columns all began from essentially the same starting community composition.

To a large extent, dominant metabolic activities in these columns were documented by geochemical measurements (e.g., nitrate and nitrite in the denitrifying columns and production of acetate and propionate at a constant ratio in the fermentative columns; Figure 1). However, nitric oxide, nitrous oxide, and ammonium were not monitored in the effluent, so geochemical evidence cannot be used to demonstrate denitrification as opposed to dissimilatory reduction of nitrate to ammonium. There is strong metatranscriptomic evidence of denitrification, however. Custom gene-expression microarrays for Hanford 100H subsurface bacteria were used to analyze RNA extracted from planktonic cells in unfiltered column effluent and revealed expression of genes associated with each of the four steps of denitrification (Figure 4A), including nitrate reductase (*narH*), nitrite reductase (*nirK*), nitric oxide reductase (*norC*), and nitrous oxide reductase (*nosZ*). One of the most highly expressed genes associated with denitrification encodes pseudoazurin, which has been reported to be a physiological electron donor for the denitrifying enzymes NirK[23] and NosZ.[24] BLASTP[25] hits of the translated versions of the denitrifying genes in Figure 4A had best matches to *Sinorhizobium* spp. (and relatives) except for NarH, which most closely matched *Pseudomonas* spp. As shown in Figure 4A, these genes are expressed at much lower (background) levels in the fermentative columns. In contrast, fermentative genes (particularly those associated with *Pelosinus* sp. strain HCF1, the dominant bacterium in the effluent) were expressed at considerably higher levels in the fermentative columns than in the denitrifying columns (Figure 4B). The genes shown in Figure 4B are all genomically located in a single gene cluster associated with the methylmalonyl-CoA pathway.[13] These genes were expressed at background levels in denitrifying columns (Figure 4B). Overall, the very different gene expression profiles shown in Figure 4 highlight the dramatic differences in metabolism in the denitrifying and fermentative columns.

Solid-Phase Analysis of Columns by Micro-X-ray Fluorescence and XAS. X-ray microprobe analysis of Cr hotspots identified in materials from all four column types was performed. Micro-XAS spectra of identified Cr hotspots showed similar spectral signatures within treatments (data not shown) and between treatment conditions (Figure 5A). Example spectra from four columns exhibiting contrasting bulk biogeochemical conditions are shown in Figure 5A. Collected spectra were compared to spectra of synthetic Cr standards (Figure 5B). The best match for the Cr XANES spectra of column precipitates was a sample made by biologically reducing Fe(III)-NTA (nitrilotriacetic acid) to Fe(II) (catalyzed by a predominant bacterial species in the

dx.doi.org/10.1021/es5016982 | Environ. Sci. Technol. XXXX, XXX, XXX–XXX

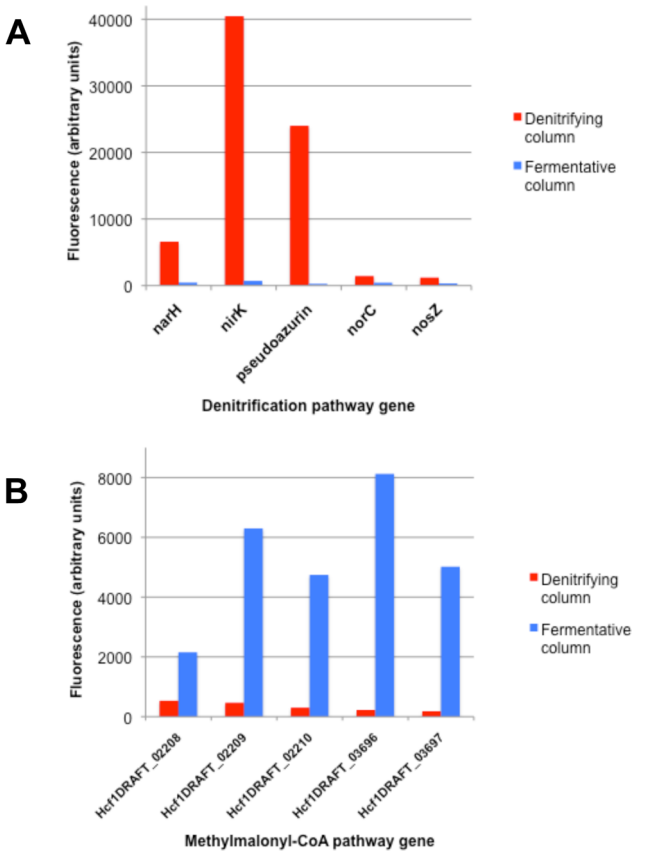

Figure 4. Expression of selected denitrification genes (A) and fermentative (methylmalonyl-CoA pathway) genes (B) in cells collected from denitrifying (red) and fermentative (blue) columns containing Hanford 100H aquifer sediment. In panel B, the best available annotations for the genes represented on the *x*-axis are as follows:[13] propionyl-CoA:succinate CoA transferase (Hcf1DRAFT_02208); methylmalonyl-CoA mutase (Hcf1DRAFT_02209−10); methylmalonyl-CoA epimerase (Hcf1DRAFT_03696); and methylmalonyl-CoA decarboxylase, α subunit (Hcf1DRAFT_03697).

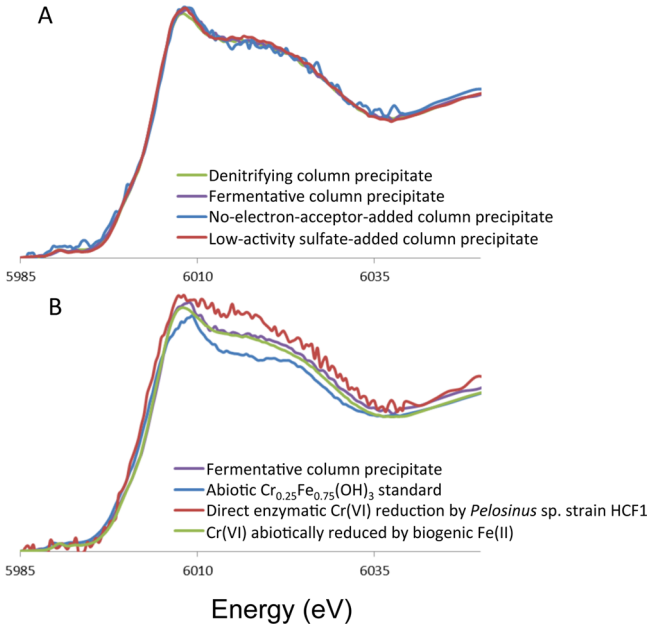

Figure 5. Cr XANES spectra of column precipitates and synthetic standards. (A) Cr XANES spectra of representative Cr spots from different column types: denitrifying, fermentative, no-electron-acceptor-added, low-activity sulfate-added. (B) Cr XANES spectra of fermentative column precipitate, abiotic $Cr_{0.25}Fe_{0.75}(OH)_3$ standard, product of direct enzymatic Cr(VI) reduction by *Pelosinus* sp. strain HCF1, and product of Cr(VI) abiotically reduced by biogenic Fe(II) that was generated by *Pelosinus* sp. strain HCF1 (see text).

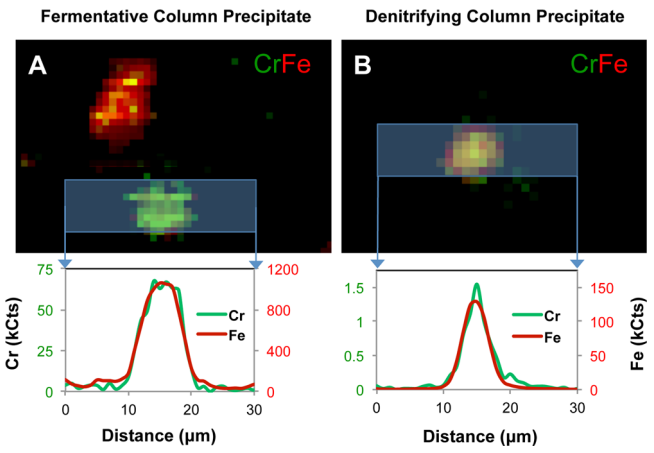

Figure 6. XRF maps of typical Cr "hotspots" from a fermentative (A) and denitrifying (B) column. Traces below images show summed detector counts for the indicated shaded areas for Cr (green) and Fe (red). Pixel size ~1 μm (A) and ~1.25 μm (B).

columns, *Pelosinus* sp. strain HCF1) and adding Cr(VI) to that mixture after heat denaturation of bacterial proteins (Figure 5B). In contrast, the spectra of $Cr_{0.25}Fe_{0.75}(OH)_3$ and $Cr(OH)_3$ (not shown) synthesized via standard hydrolysis methods, and of enzymatically reduced Cr(VI), did not closely match the spectral shape of the column precipitates. Comparison of data from the $Cr_{0.5}Fe_{0.5}(OH)_3$ standard used here with data from previous work[26] indicated that our standard was closely comparable (F. Marc Michel, personal communication), and therefore the mismatch between the column precipitates and our hydrolysis standards was not an artifact of our synthesis methods but rather a real difference between the column precipitates and hydrolysis standards.

Fine-scale X-ray fluorescence maps of two example Cr hotpots are shown in Figure 6. The Gaussian distribution of line traces of Cr and Fe fluorescence, as opposed to higher Cr content at the edges, implies a material that is uniform on the scale of analysis rather than a coating. As can be seen by the divergent *y*-axis scales, the Fe fluorescence from particles was significantly greater than that of the Cr. Of the 19 particles analyzed (12 from a fermentative column and 7 from a denitrifying column), most showed low Cr-to-Fe fluorescence ratios as represented in Figure 6. The highest Cr-to-Fe fluorescence ratio recorded was ~0.37 which, although the detected fluorescence yields are not directly comparable to atomic compositions, is consistent with the 0.33 stoichiometric ratio expected for Cr(VI) reduction by Fe(II). The size of the particles, ~10 and ~5 μm (fwhm, or full width at half-maximum) for fermentative and denitrifying columns, respectively, was typical, although some were as a large as ~20 μm (fwhm).

Additional solid-phase analysis (by micro-XANES) shows the presence of reduced sulfur-containing precipitates in the fermenting columns (Supporting Information, Figure S7) consistent with S(-II) to S(0). Thus, despite the weak evidence

dx.doi.org/10.1021/es5016982 | Environ. Sci. Technol. XXXX, XXX, XXX−XXX

of sulfate reduction in fermentative columns based on effluent data (Figure 1D), there was some degree of sulfate reduction taking place in these columns. Also, a few spots in the denitrifying column showed evidence for some residual Cr(VI) (<5% of total Cr) (Supporting Information, Figure S8), suggesting a slower net Cr(VI) reduction rate in the denitrifying columns relative to the fermentative columns (as also indicated in Figure 1).

Chromate Reduction Mechanism: Competing Evidence for Enzymatic Reduction versus Chemical Reduction by Biogenic Fe(II). The preceding geochemical and biological data suggest two different scenarios for microbially mediated Cr(VI) reduction that might explain how two such different biogeochemical regimes (denitrifying and fermentative) could result in very similar Cr(III)−Fe(III) mineral phases: scenario I is enzymatic reduction of Cr(VI) to Cr(III) followed by coprecipitation of Cr(III) and Fe(III); scenario II is that both regimes generated at least small amounts of Fe(II) (solid-phase and/or dissolved-phase), which abiotically reduced Cr(VI) to form a Cr−Fe precipitate. There are competing lines of evidence that support and undermine each scenario.

Evidence favoring scenario I (enzymatic reduction) includes the following: (a) Hanford 100H bacterial isolates have been shown to reduce Cr(VI) in systems without Fe, and the species that dominated the fermenting columns (*Pelosinus* sp. strain HCF1) has a higher Cr(VI) reduction rate than Hanford 100H denitrifying bacteria tested to date,[12,13] which is consistent with the faster rates observed in fermentative columns than in denitrifying columns (Figure 1); (b) highly correlated chromate and nitrate consumption rates (Supporting Information, Figure S2) are consistent with cometabolic chromate reduction,[12] which would support an enzymatic mechanism in the denitrifying columns; (c) the observed Cr−Fe hydroxide precipitate is a thermodynamically stable phase.[27] Evidence arguing against scenario I includes the very low solubility (and consequently low availability) of Fe(III) to interact with Cr(III), and the observation that synthetic mixtures of Fe(III) and Cr(III) did not yield XANES spectra comparable to the spectra observed for the column precipitates (Figure 5).

Evidence favoring scenario II [abiotic reduction by Fe(II)] includes the following: (a) good agreement between XANES spectra from columns and standards made by allowing the chemical reaction of Cr(VI) with a biogenic Fe(II) phase (Figure 5); (b) the generally much faster rates of chromate reduction when Fe(II) is the chemical reductant relative to enzymatically catalyzed reactions [e.g., we estimate that just a 50 nM concentration of Fe(II) would reduce Cr(VI) at the same rate as enzymatic reduction by *Pelosinus* sp. strain HCF1 at the relatively high cell density of 10^7 cells/mL; Figure S9]. Evidence undermining scenario II includes the thermodynamic unfavorability of Fe(III) reduction under nitrate-reducing conditions [in fact, Fe(II) oxidation would be favored]. On the basis of geochemical (nitrate, nitrite; Figure 1B) data and gene expression data (Figure 4A), nitrate reduction clearly was occurring in the nitrate-amended columns throughout the study.

Do Bulk Biogeochemical Data Provide Insufficient Evidence To Infer Processes Occurring at Much Smaller Scales? The data we have presented do not definitively favor either of the scenarios described above. There is, however, another factor in data interpretation that could help to reconcile the apparent contradiction between the two scenarios: the scale of the observations (e.g., bulk data versus the role of local-scale heterogeneity). More specifically, a major argument against the role of biological Fe(III) reduction in a denitrifying regime is that the process would be thermodynamically unfavorable. Bulk (whole-column) effluent measurements from the denitrifying columns showing the continuous presence of nitrite and lactate (and typically also nitrate) throughout the 1-year experiment (Figure 1B), and bulk (whole-column) metatranscriptomic evidence of expression of denitrifcation genes (Figure 4A), all suggest a continuously denitrifying regime in which Fe(III) reduction should never occur. However, if there were local areas in the columns in which nitrate was sufficiently depleted, Fe(III) reduction could be more thermodynamically favorable in such zones. As shown in Figure 2A, biogeochemical activity was clearly not uniform throughout the columns. Cr(VI) reduction (precipitation) was greater at the head (inlet) of the column in the fermenting and denitrifying columns, and Fe(III) reduction was also clearly greater at the head of the fermenting columns. Also, the importance of small-scale conditions (e.g., microenvironments) could be magnified in this study because only a very small fraction of the reducing equivalents from the electron donor (5 mM lactate) would be needed to reduce the relatively small amount of Cr(VI) in the influent (5 μM). Thus, even if a very small portion of reducing equivalents were being used to reduce Fe(III) in nondenitrifying microenvironments, this might account for a substantial portion of the Cr(VI) reduced overall. (Note that, although the Cr(VI) concentrations in this study were low in molar terms, they still were environmentally relevant and exceeded U.S. EPA Maximum Contaminant Levels by 2.6-fold.)

None of the foregoing discussion definitively shows why such similar Cr−Fe precipitates were formed in two such different biogeochemical regimes, but it does suggest that, even in relatively small-scale systems, bulk biogeochemical data may not provide sufficient evidence to infer processes dominated by microenvironments. Extrapolating the results of this study to the field scale suggests that interpretations of dominant processes controlling Cr(VI) reduction could be impeded to a great extent by bulk measurements. It is not practical to recommend fine-scale measurements for field studies of intrinsic or engineered Cr(VI) reduction, but there are lessons from this laboratory study that would be beneficial in interpreting future field and laboratory studies of biologically mediated Cr(VI) reduction: (a) independent of bulk biogeochemical conditions, it appears that reduced Cr may ultimately occur in mixed Cr−Fe precipitates, (b) even if known microbes or genes associated with biotic Fe(III) reduction are not detected in the system based on bulk biological measurements (i.e, phylogenetic, metagenomic, metatranscriptomic, or metaproteomic data), there still might be sufficient biogenic Fe(II) produced to mediate Cr(VI) reduction, and (c) overall, the bulk redox status and biogeochemical regime, as categorized by the dominant electron-accepting process, do not necessarily control the final product of Cr(VI) reduction, as the product was the same (Figures 5A and 6) even though the bulk conditions were very different (Figures 1A−D, 3, and 4) .

■ ASSOCIATED CONTENT

Supporting Information

Description of gene expression microarray design; effluent data for individual flow-through columns; solid-phase Cr data from

dx.doi.org/10.1021/es5016982 | Environ. Sci. Technol. XXXX, XXX, XXX−XXX

four column types; micro XANES spectra of S-containing precipitates; and a summary kinetic comparison between abiotic Cr(VI) reduction with Fe(II) versus direct enzymatic Cr(VI) reduction. This material is available free of charge via the Internet at http://pubs.acs.org.

AUTHOR INFORMATION

Corresponding Author

*Phone: (510) 486-7118; fax: (510) 486-5686; e-mail: PSNico@lbl.gov.

Notes

The authors declare no competing financial interest.

ACKNOWLEDGMENTS

We thank Joern Larsen and Boris Faybishenko for assistance with ICP−MS analysis and collection of aquifer materials, respectively. This work was supported as part of the Subsurface Biogeochemical Research Scientific Focus Area funded by the U.S. Department of Energy, Office of Science, Office of Biological and Environmental Research under Award Number DE-AC02-05CH11231. The operations of Beamline 10.3.2 at the Advanced Light Source at Lawrence Berkeley National Laboratory are also supported by the Director, Office of Science, Office of Basic Energy Sciences, U.S. Department of Energy under contract number DE-AC02-05CH11231.

REFERENCES

(1) Costa, M.; Klein, C. B. Toxicity and carcinogenicity of chromium compounds in humans. *Crit. Rev. Toxicol.* **2006**, *36* (2), 155−163.

(2) Cieslak-Golonka, M. Toxic and mutagenic effects of chromium-(VI). A review. *Polyhedron* **1996**, *15* (21), 3667−3689.

(3) *Cleaning up the Nations Waste Sites: Markets and Technology Trends*; EPA 542-R-96-005; U.S. Environmental Protection Agency: Washington, DC, 1996.

(4) Cheung, K.; Gu, J.-D. Mechanism of hexavalent chromium detoxification by microorganisms and bioremediation application potential: A review. *Int. Biodeterior. Biodegrad.* **2007**, *59*, 8−15.

(5) Ramirez-Diaz, M. I.; Diaz-Perez, C.; Vargas, E.; Riveros-Rosas, H.; Campos-Garcia, J.; Cervantes, C. Mechanisms of bacterial resistance to chromium compounds. *Biometals* **2008**, *21* (3), 321−32.

(6) Fendorf, S.; Wielinga, B. W.; Hansel, C. M. Chromium transformations in natural environments: The role of biological and abiological processes in chromium(VI) reduction. *Int. Geol. Rev.* **2000**, *42*, 691−701.

(7) Dai, R.; Liu, J.; Yu, C.; Sun, R.; Lan, Y.; Mao, J. D. A comparative study of oxidation of Cr(III) in aqueous ions, complex ions, and insoluble compounds by manganese-bearing mineral (birnessite). *Chemosphere* **2009**, *76* (4), 536−541.

(8) Oze, C.; Bird, D. K.; Fendorf, S. Genesis of hexavalent chromium from natural sources in soil and groundwater. *Proc. Natl. Acad. Sci. U.S.A.* **2007**, *104* (16), 6544−6549.

(9) Rajapaksha, A. U.; Vithanage, M.; Ok, Y. S.; Oze, C. Cr(VI) Formation related to Cr(III)-muscovite and birnessite interactions in ultramafic environments. *Environ. Sci. Technol.* **2013**, *47* (17), 9722−9729.

(10) Faybishenko, B.; Hazen, T. C.; Long, P. E.; Brodie, E. L.; Conrad, M. E.; Hubbard, S. S.; Christensen, J. N.; Joyner, D.; Borglin, S. E.; Chakraborty, R.; et al. In situ long-term reductive bioimmobilization of Cr(VI) in groundwater using Hydrogen Release Compound. *Environ. Sci. Technol.* **2008**, *42* (22), 8478−8485.

(11) Dresel, P. E.; Ainsworth, C. C.; Qafoku, N. P.; Liu, C.; McKinley, J. P.; Itlton, E. S.; Fruchter, J. S.; Phillips, J. L. *Geochemical Characterization of Chromate Contamination in the 100 Area Vadose Zone at the Hanford Site.*; Report PNNL-17674; Pacific Northwest National Laboratory: Richland, WA, 2008.

(12) Han, R.; Geller, J. T.; Yang, L.; Brodie, E. L.; Chakraborty, R.; Larsen, J. T.; Beller, H. R. Physiological and transcriptional studies of Cr(VI) reduction under aerobic and denitrifying conditions by an aquifer-derived pseudomonad. *Environ. Sci. Technol.* **2010**, *44* (19), 7491−7.

(13) Beller, H. R.; Han, R.; Karaoz, U.; Lim, H.; Brodie, E. L. Genomic and physiological characterization of the chromate-reducing, aquifer-derived Firmicute *Pelosinus* sp. strain HCF1. *Appl. Environ. Microbiol.* **2013**, *79* (1), 63−73.

(14) Ivanov, I. I.; Atarashi, K.; Manel, N.; Brodie, E. L.; Shima, T.; Karaoz, U.; Wei, D.; Goldfarb, K. C.; Santee, C. A.; Lynch, S. V.; Tanoue, T.; Imaoka, A.; Itoh, K.; Takeda, K.; Umesaki, Y.; Honda, K.; Littman, D. R. Induction of intestinal Th17 cells by segmented filamentous bacteria. *Cell* **2009**, *139* (3), 485−98.

(15) Lovley, D. R.; Phillips, E. J. Rapid assay for microbially reducible ferric iron in aquatic sediments. *Appl. .Environ. Microbiol.* **1987**, *53* (7), 1536−40.

(16) Stookey, L. Ferrozine—A new spectrophotometric reagent for iron. *Anal. Chem.* **1970**, *42* (7), 779−781.

(17) Ravel, B.; Newville, M. ATHENA, ARTEMIS, HEPHAESTUS: Data analysis for X-ray absorption spectroscopy using IFEFFIT. *J. Synchrotron Radiat.* **2005**, *12* (Pt 4), 537−41.

(18) Caporaso, J. G.; Kuczynski, J.; Stombaugh, J.; Bittinger, K.; Bushman, F. D.; Costello, E. K.; Fierer, N.; Pena, A. G.; Goodrich, J. K.; Gordon, J. I.; et al. QIIME allows analysis of high-throughput community sequencing data. *Nat. Methods* **2010**, *7* (5), 335−6.

(19) Bouskill, N. J.; Lim, H. C.; Borglin, S.; Salve, R.; Wood, T. E.; Silver, W. L.; Brodie, E. L. Pre-exposure to drought increases the resistance of tropical forest soil bacterial communities to extended drought. *ISME J.* **2013**, *7* (2), 384−94.

(20) R Core Team. *R: A language and Environment for Statistical Computing*; R Foundation for Statistical Computing: Vienna, Austria, 2013.

(21) Rajeev, L.; da Rocha, U. N.; Klitgord, N.; Luning, E. G.; Fortney, J.; Axen, S. D.; Shih, P. M.; Bouskill, N. J.; Bowen, B. P.; Kerfeld, C. A.; et al. Dynamic cyanobacterial response to hydration and dehydration in a desert biological soil crust. *ISME J.* **2013**, *7* (11), 2178−91.

(22) Konovalova, V.; Nigmatullin, R.; Dmytrenko, G.; Pobigay, G. Spatial sequencing of microbial reduction of chromate and nitrate in membrane bioreactor. *Bioprocess Biosyst. Eng.* **2008**, *31* (6), 647−53.

(23) Kukimoto, M.; Nishiyama, M.; Tanokura, M.; Adman, E. T.; Horinouchi, S. Studies on protein−protein interaction between copper-containing nitrite reductase and pseudoazurin from *Alcaligenes faecalis* S-6. *J. Biol. Chem.* **1996**, *271* (23), 13680−3.

(24) Fujita, K.; Hirasawa-Fujita, M.; Brown, D. E.; Obara, Y.; Ijima, F.; Kohzuma, T.; Dooley, D. M. Direct electron transfer from pseudoazurin to nitrous oxide reductase in catalytic N_2O reduction. *J. Inorg. Biochem.* **2012**, *115*, 163−73.

(25) Altschul, S. F.; Madden, T. L.; Schaffer, A. A.; Zhang, J.; Zhang, Z.; Miller, W.; Lipman, D. J. Gapped BLAST and PSI-BLAST: A new generation of protein database search programs. *Nucleic Acids Res.* **1997**, *25* (17), 3389−402.

(26) Tang, Y.; Michel, F. M.; Zhang, L.; Harrington, R.; Parise, J. B.; Reeder, R. J. Structural properties of the Cr(III)−Fe(III) (oxy)-hydroxide compositional series: Insights for a nanomaterial "solid solution". *Chem. Mater.* **2010**, *22* (12), 3589−3598.

(27) Sass, B. M.; Rai, D. Solubility of amorphous chromium(III)−iron(III) hydroxide solid solutions. *Inorg. Chem.* **1987**, *26* (14), 2228−2232.

NOTE ADDED AFTER ASAP PUBLICATION

This paper was published on the Web on August 13, 2014, with an error in the first paragraph. The corrected version was reposted on August 14, 2014.